Computational and Structural Biotechnology Journal 23 (2024) 4131–4142

Contents lists available at ScienceDirect

Computational and Structural Biotechnology Journal

journal homepage: www.elsevier.com/locate/csbj

Research article

Transcriptome-based characterization of 3'2'-cGAMP signaling mediated immune responses

Yan Gao [a,b,1], Gucheng Xu [c,1], Munire Maimaiti [b,1], Saihua Chen [b], Xiang Zhang [b], Jiameng Hu [a,b], Chen Wang [b,*], Ze Hong [c,*], Haiyang Hu [a,b,d,**]

[a] Central Laboratory, Shanghai Pulmonary Hospital, Tongji University School of Medicine, Shanghai, China
[b] State Key Laboratory of Natural Medicines, School of Life Science and Technology, China Pharmaceutical University, Nanjing, China
[c] School of Pharmacy, Nanjing University of Chinese Medicine, Nanjing, China
[d] Chongqing Innovation Institute of China Pharmaceutical University, Chongqing, China

ARTICLE INFO

Keywords:
3'2'-cGAMP signaling
2'3'-cGAMP signaling
STING
Transcriptome
Adjuvant

ABSTRACT

Cyclic dinucleotides (CDNs) are critical adjuvants in antiviral vaccines and cancer immunotherapy, primarily through the activation of the cGAS-STING signaling pathway. Evaluating the immune responses triggered by CDNs is essential for the development of effective adjuvants. In this study, we performed a comparative transcriptome analysis to characterize the immune responses elicited by the recently identified nuclease-resistant Drosophila and bacterial CDN, 3'2'-cGAMP, in mammalian immune cells. We detected a robust induction of innate immune gene signature following 3'2'-cGAMP stimulation in digitonin-permeabilized mouse primary macrophages, comparable to the response observed with the canonical mammalian CDN, 2'3'-cGAMP. STING deficiency remarkably reduced 3'2'-cGAMP-induced phosphorylation of TBK1 and IRF3 and the induction of IFN-β, indicating that 3'2'-cGAMP signaling-mediated immune responses were mainly STING dependent. In comparison to 2'3'-cGAMP signaling, 3'2'-cGAMP signaling preferentially elicited many STING-dependent genes involved in transcription and nucleosome positioning and assembly in the nucleus, which are likely associated with several enriched pathways, including cellular senescence, HDACs deacetylate histones, and epigenetic regulation of gene expression. The integrative analysis further revealed that 3'2'-cGAMP signaling preferentially induced genes were associated with autoimmune disease-related processes, suggesting a potential side effect that requires monitoring when used as an adjuvant. In conclusion, this study provides the first transcriptional landscape of 3'2'-cGAMP signaling in mammals and reveals the immune response characteristics and potential side effects mediated by 3'2'-cGAMP signaling. These findings may aid in the development of 3'2'-cGAMP-based adjuvants for antiviral vaccines and cancer immunotherapy.

1. Introduction

The cGAS-STING pathway is an evolutionarily conserved immune signaling pathway [1,2]. Among the agonists of the cGAS-STING pathway, cyclic dinucleotides (CDNs) are the most important natural agonists for activating the cGAS-STING pathway[3,4]. Well-known bacterial CDNs include c-di-AMP, c-di-GMP, and 3'3'-cGAMP [5]. In mammals, the most prominent CDN is 2'3'-cGAMP. All these CDNs can activate the cGAS-STING pathway in mammals by binding and activating the endoplasmic reticulum-associated transmembrane protein STING (stimulator of IFN gene)[4]. Activated STING phosphorylates TBK1 kinase to trigger IRF3-dependent innate immune responses, including IFN-β induction and the activation of interferon-stimulated genes (ISGs) [2,6], along with many IRF3-independent effectors, which vary based on cellular context and signaling duration [7–10].

The cGAS-STING pathway was first identified as crucial for antiviral immunity and antimicrobial defense [1,2]. Recently, growing evidence has highlighted the critical role of the cGAS-STING pathway in antiviral vaccines and cancer immunotherapy [3,11,12]. The type I IFN signature of the cGAS-STING pathway is essential for enhancing antigen-specific T

* Corresponding authors.
** Corresponding author at: State Key Laboratory of Natural Medicines, School of Life Science and Technology, China Pharmaceutical University, Nanjing, China.
E-mail addresses: cwang1971@cpu.edu.cn (C. Wang), 300575@njucm.edu.cn (Z. Hong), haiyanghu@cpu.edu.cn (H. Hu).
[1] These authors contributed equally to this work

https://doi.org/10.1016/j.csbj.2024.11.021
Received 22 September 2024; Received in revised form 8 November 2024; Accepted 9 November 2024
Available online 12 November 2024

cell responses and natural killer cell responses, which together drive cell-mediated immunity. In specific cellular contexts, the cGAS-STING pathway can induce several forms of programmed cell death, including apoptosis, necroptosis, and lysosomal cell death. The versatility of the cGAS-STING pathway enables immune responses that can ultimately clear virus and tumor cells. Given its importance in enhancing immune responses, recent research has focused on CDNs or their mimics as adjuvants in antiviral vaccines and cancer immunotherapy. CDN-adjuvanted protein subunit vaccines protect mice from respiratory bacterial and viral infections such as *Mycobacterium tuberculosis*, *Influenza, anthrax*, *Acinetobacter baumannii*, *Klebsiella pneumoniae* and *Streptococcus pneumoniae*, and methicillin-resistant *Staphylococcus aureus*[12–18]. CDNs have also exhibited promising therapeutic effects in cancer immunotherapy in mice. For instance, intraperitoneal injection of bacterial c-di-GMP overcomes immune suppression and improves vaccine efficacy against metastatic breast cancer in the 4T1 murine model [19]. Treatment of the bacterial c-di-GMP inhibits both basal and growth factor (acetylcholine and epidermal growth factor)-induced cell proliferation of human colon cancer (H508) cells [20]. Intertumoral vaccination with mammalian 2'3'-cGAMP remodels the tumor immune microenvironment by repolarizing M2-like tumor-associated macrophages into antitumor M1-type macrophages in HSC-2 squamous cell carcinomas, CT26 murine colon cancer, and B16F10 murine melanoma [21]. These observations indicate significant potential for CDNs as STING agonists in antiviral vaccines and tumor immunotherapy, despite most CDNs being bacterial in origin and not naturally occurring in humans. However, known natural CDNs are susceptible to nuclease degradation and often exhibit unwanted toxicities. Thus, there is a great need to evaluate newly identified CDNs for their potential as adjuvants.

3'2'-cGAMP is a recently identified CDN in Drosophila and bacteria that plays a role in immune responses[22–24]. 3'2'-cGAMP is synthesized by cGLR (cGAS-like receptors), which is crucial for the protection from viral infection in Drosophila melanogaster [22]. Additionally, 3'2'-cGAMP is resistant to nucleases that degrade 2'3'-cGAMP, thereby preserving STING-dependent immunity [22]. Intriguingly, overexpression of cGLR with poly (I:C) stimulation led to STING activation in human HEK cells [22], suggesting the potential of 3'2'-cGAMP as a STING agonist in mammalian species. However, no systematic analysis of 3'2'-cGAMP-mediated immune responses has yet been performed in mammals. To evaluate the potential of 3'2'-cGAMP as an adjuvant, initial studies are needed to determine whether 3'2'-cGAMP can induce immune responses in mouse immune cells and to characterize these responses. Characterizing 3'2'-cGAMP-mediated immune responses in mouse cells through comparative transcriptome analysis with canonical 2'3'-cGAMP would aid in evaluating 3'2'cGAMP as an adjuvant in antiviral vaccines and cancer immunotherapy.

In this study, we conducted a comparative transcriptome analysis to examine the potential immune responses induced by the 3'2'-cGAMP signaling activation in mouse primary macrophages. RNA-Seq analysis revealed strong activation of innate immune-related genes at 3 h and 9 h post 3'2'-cGAMP signaling activation, similar to responses triggered by the canonical mammalian CDN 2'3'-cGAMP. STING ablation notably reduced 3'2'-cGAMP-induced phosphorylation of TBK1 and IRF3, as well as IFN-β expression, indicating that 3'2'-cGAMP-mediated immune responses in mice are strongly STING-dependent. Compared to 2'3'-cGAMP signaling, 3'2'-cGAMP preferentially prompted the activation of many genes associated with transcription and nucleosome positioning and assembly in the nucleus, in a STING-dependent manner. We also found that 3'2'-cGAMP signaling preferentially induced genes significantly linked to the autoimmune disease SLE, suggesting potential adverse effects of 3'2'-cGAMP as an adjuvant. In summary, our study presents the first transcriptional profile of 3'2'-cGAMP signaling in mouse macrophages, revealing immune response characteristics and potential adverse effects that could inform the development of 3'2'-cGAMP-based adjuvants for antiviral vaccines and cancer immunotherapy.

2. Materials and methods

2.1. Mice and ethics statement

Sting$^{-/-}$ (*Sting*-deficient) mice of C57BL/6 J background were kindly provided by Dr. Zhengfan Jiang (Peking University) and genotyped using the following primers: Forward TGCTGTAGGATGCTATGTGC; Reverse CAGTCCAGGTAACCCTCTGT. The wild-type mice of C57BL/6 J background were purchased from the Model Animal Research Center of Nanjing University. All mice were maintained under the specific pathogen-free (SPF) conditions at the Center for New Drug Safety Evaluation and Research, China Pharmaceutical University. All mice experiments were performed in accordance with the National Institutes of Health Guide for the Care and Use of Laboratory Animals, with the approval of the Center for New Drug Safety Evaluation and Research, China Pharmaceutical University (Approval Number 2022–04–002). A total of fifteen wild-type male mice and Fifteen *Sting*$^{-/-}$ male mice, aged 8 to 12 weeks, were used in our experiments, including six wild-type male mice and six *Sting*$^{-/-}$ male mice used for RNA-Seq experiments, and nine wild-type male mice and nine *Sting*$^{-/-}$ male mice used for Real-time PCR, ELISA, and Western blot experiments.

2.2. Cell culture

To obtain bone marrow-derived macrophages (BMDMs) of mice, femurs were aseptically harvested from wild-type and *Sting*$^{-/-}$ mice. Bone marrow cells were then flushed from the bones and then cultured in the RPMI 1640 media (20 % FBS, 50 μM 2-mercaptoethanol, 2 mM L-glutamine) with 40 ng/mL macrophage colony-stimulating factor (M-CSF). The medium was refreshed every two days, and the cells were differentiated to BMDMs within week. BMDMs were kept individually for each mouse and maintained in a humidified 5 % CO_2 incubator at 37 °C.

2.3. Experiments of 3'2'-cGAMP and 2'3'-cGAMP stimulation

For the RNA-Seq profiling, the stimulation experiments were conducted in biological replicates with 2'3'-cGAMP or 3'2'-cGAMP stimulation, as shown in Fig. 1A. Briefly, based on individually kept BMDMs isolated from six wild-type mice, we firstly permeabilized them for 30 min with digitonin buffer (10 μg/mL digitonin, 50 mM HEPES-KOH pH 7.5, 100 mM KCl, 3 mM $MgCl_2$, 0.1 mM DTT, 85 mM sucrose, 0.2 % BSA, 1 mM ATP, and 0.1 mM GTP). Next, two of these BMDMs were treated with 3'2'-cGAMP for 3 h and 9 h, and another two with 2'3'-cGAMP for 3 h and 9 h. The remaining two digitonin permeabilized BMDMs, without 3'2'-cGAMP or 2'3'-cGAMP treatment, served as mock controls. For each stimulation, 1 μg/mL of synthesized 3'2'-cGAMP or 2'3'-cGAMP was delivered into the cultured BMDMs via digitonin permeabilization as previously described [25]. The same procedure was applied to individually kept BMDMs isolated from six *Sting*$^{-/-}$ mice. This experimental design yielded 24 BMDM samples for RNA-Seq experiment. For the Real-time PCR, ELISA, and Western blot experiments, stimulation experiments were conducted in three biological replicates with 2'3'-cGAMP or 3'2'-cGAMP stimulation, based on individually kept BMDMs isolated from nine wild-type male mice and nine *Sting*$^{-/-}$ male mice.

2.4. RNA-Seq experiment

We conducted the RNA-Seq experiment based on 24 BMDM samples in biological replicates from 3'2'-cGAMP and 2'3'-cGAMP stimulation experiments, yielding 24 RNA-Seq datasets. The RNA-Seq experiment was conducted as previously described [25–27]. In brief, total RNA was extracted using the TRIzol reagent (Invitrogen) from the digitonin-permeabilized BMDM cells, followed by polyA RNA enrichment with the TruSeq RNA Library Preparation Kit v2 (Illumina). The

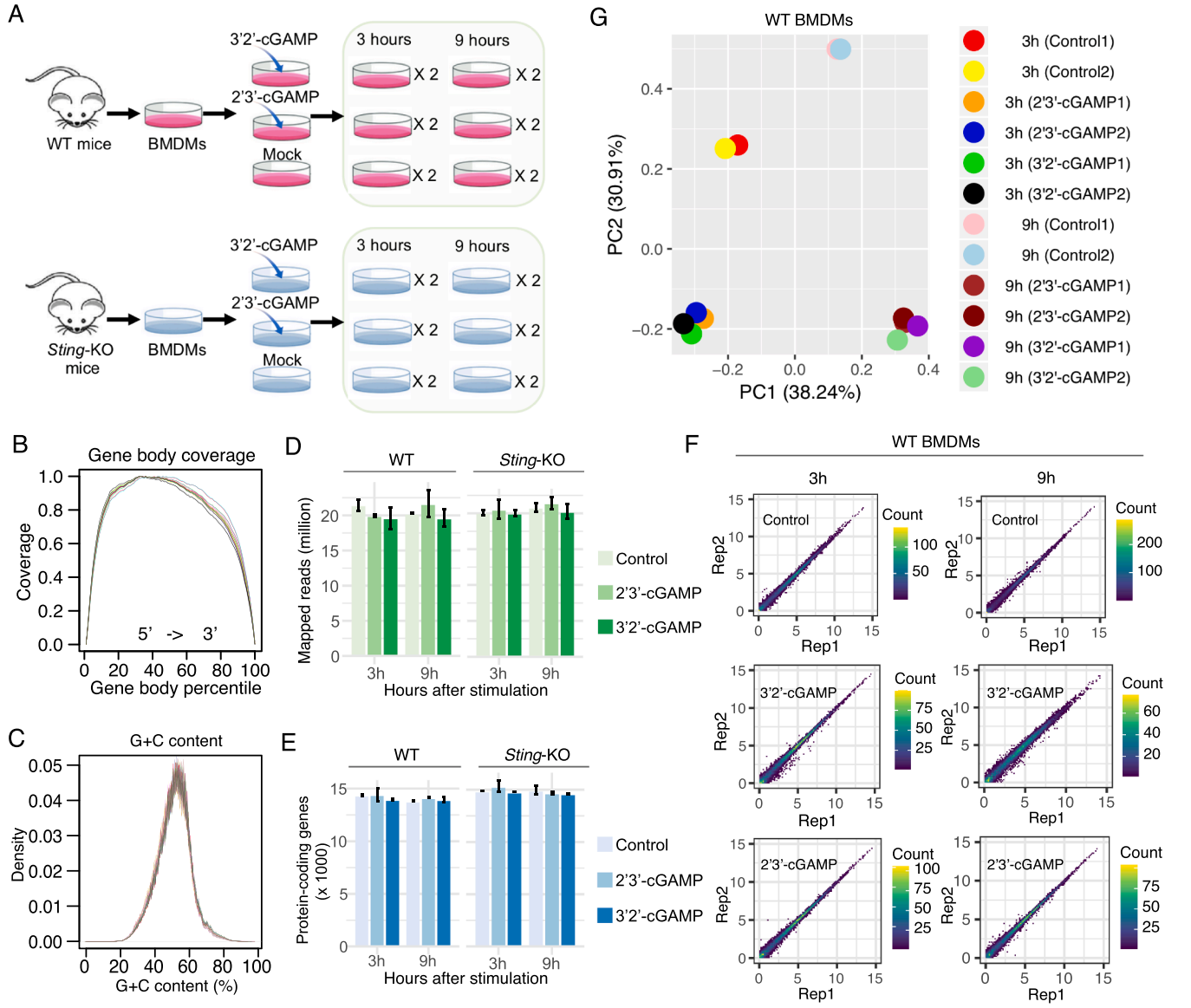

Fig. 1. Overall experimental design and RNA-Seq data quality assessment. (A) Schematic of experimental design and sample collection for RNA-Seq, showing activation of 3'2'-cGAMP and 2'3'-cGAMP signaling in biological replicates at 3 and 9 h. Isolated BMDMs were kept individually for each mouse and were digitonin permeabilized before stimulation with 3'2'-cGAMP, 2'3'-cGAMP, or mock treatment. The stimulation experiments were conducted in biological replicates, denoted as "X 2" in the schematic (See Methods). (B) Read coverage distribution along the transcript body of annotated protein-coding genes in each RNA-Seq sample. (C) G+C content per RNA-Seq sample. (D) Barplot of the number of mapped paired-end reads per RNA-Seq sample. (E) Barplot of the number of quantified paired-end reads per RNA-Seq sample. (F) Scatter density plot of expression abundance for protein-coding genes between replicates in WT BMDMs. (G) PCA plot showing RNA-Seq sample clustering in WT BMDMs.

enriched RNA was then converted into cDNA libraries according to Illumina's traditional RNA-Seq protocol. Prior to library construction, RNA integrity was assessed using the RIN (RNA Integrity Number) value with an Agilent 2100 system, and only samples with a RIN of at least nine were selected for library preparation. The cDNA libraries were then sequenced on an Illumina HiSeq2500 platform using the 2 × 150 nt paired-end configuration.

2.5. RNA-Seq data analysis

Based on 24 RNA-Seq data in biological replicates, the RNA-Seq data analysis was followed as previously described [25–28]. Specifically, raw sequencing data from the 24 RNA-Seq samples were preprocessed using Trimmomatic [29] to remove potential adaptor contamination and low-quality reads. The obtained reads over 75 nt were further processed using FastQC to inspect overall read quality regarding read sequencing base quality, read G+C content, and adaptor contamination. MultiQC [30] was used to visualize read G+C content and the read sequencing quality in the format of the average Phred score of each base. The high-quality reads were aligned to the mouse genome (mm10) using HISAT2 [31] with default parameters for gene expression quantification. Only uniquely mapped reads were retained to estimate gene expression abundance at the count level using featureCounts [32]. The mouse genome was downloaded from the FTP of the Ensembl database (ftp://ftp.ensembl.org/pub). The mouse reference gene annotation in GTF format was downloaded from the FTP of the Ensembl database (ftp://ftp.ensembl.org/pub). The gene body coverage of mapped reads was estimated based on the script 'geneBody_coverage.py' of the RSeQC package [33], using the transcripts of all annotated protein-coding genes as the template. We applied TMM (Trimmed Mean of M-values)

normalization method to adjust for differences in RNA sequencing library size and RNA composition between RNA-Seq samples. The TMM normalization method, implemented in edgeR [34], calculates scaling factors based on a weighted trimmed mean of the log-expression ratios, which is robust against differences in RNA sequencing library size and RNA composition between samples. Differentially expressed (DE) genes in response to 3'2'-cGAMP stimulation at 3 h were identified using edgeR, comparing two 3'2'-cGAMP samples with two mock controls under a false discovery rate (FDR) threshold of 0.05. The same procedure was applied to obtain DE genes for the conditions of 3'2'-cGAMP stimulation at 9 h, 2'3'-cGAMP stimulation at 3 h, and 2'3'-cGAMP stimulation at 9 h.

2.6. Enrichment analysis

The gene ontology (GO) and pathway enrichment analysis were performed using David Bioinformatics (https://david.ncifcrf.gov/). The significantly enriched items were obtained based on the FDR cutoff of less than 0.1. All expressed genes were used as the background set.

2.7. Chromosome location enrichment analysis

Chromosomal location enrichment analysis was performed using Fisher's exact test. Specifically, for a given gene set, the number of genes on each chromosome was counted, and enrichment on each chromosome was assessed by comparing this count to the gene count on all other chromosomes using Fisher's exact test. The resulting p-values were adjusted using the Benjamini-Hochberg (BH) procedure, with a BH-adjusted p-value < 0.05 considered significant.

2.8. Transcriptome analysis after estrogen treatment based on public data

We downloaded the public gene expression microarray data from mouse macrophage cell line (raw264.7 cells) before and after estrogen treatment to examine the gene expression changes of 3'2'-cGAMP signaling preferentially induced genes following estrogen exposure. This experiment, conducted by Zhang et al. [35], involved treating raw 264.7 cells with and without 1 μg/mL estrogen overnight before microarray profiling [35]. The dataset was obtained from NCBI's GEO (accession number GSE52649) and quantified into a gene expression matrix using the RMA package [36]. This analysis was conducted for two reasons: (1) we identified an association between 3'2'-cGAMP signaling-induced genes and the autoimmune disease SLE, and (2) estrogen is a known risk factor for SLE pathogenesis [37].

2.9. Blood transcriptome analysis of SLE cohorts based on public data

To investigate changes in the expression of genes induced and preferentially induced by 3'2-cGAMP signaling in the blood of SLE patients, we analyzed gene expression profiles from three independent SLE cohorts. These cohorts included: SLE cohort-1 with 20 SLE patients and 6 healthy donors (GSE122459, RNA-Seq data), SLE cohort-2 with 127 SLE patients and 20 healthy donors (GSE49454, microarray data), and SLE cohort-3 with 924 SLE patients and 48 healthy donors (GSE65391, microarray data).

2.10. Transcriptome analysis after 2'3'-cGAMP stimulation using public data

We examined the expression changes of 3'2-cGAMP signaling preferentially induced genes before and after 2'3'-cGAMP stimulation using public data from GSE142735.

2.11. Catalog of interferon-stimulated genes (ISGs)

We collected known human and mouse interferon-stimulated genes (ISGs) from [38]. Mouse orthologs of human ISGs were identified using Ensembl Compara via the BioMart database [39]. The ISG catalog used in this study comprised a merged list of known mouse ISGs and mouse orthologs of human ISGs.

2.12. Simulation analysis

To determine whether the correlation of expression changes in differentially expressed genes between WT and *Sting*-deficient BMDMs after 3'2-cGAMP stimulation differed from that of all expressed genes, we randomly selected a set of genes from all expressed genes, matching the number of differentially expressed genes. We then calculated the correlation of expression changes between WT and *Sting*-deficient BMDMs following 3'2-cGAMP stimulation. This procedure was repeated 1000 times, and the resulting correlation distribution was used as the null distribution to assess the significance of the correlation in the differentially expressed genes.

2.13. Real-time PCR

Total RNA was isolated using TRIzol reagent according to the manufacturer's instructions, and then subjected to reverse transcription using oligo (dT) primers. The quantification of gene transcripts was performed by real-time PCR with ChamQ SYBR qPCR Master Mix using QuantStudio 3 Real-Time PCR System. The induction of interferon-stimulated genes (ISGs) is a hallmark of the activation of innate immunity[26], and therefore we selected three well-known ISGs (*Mx1, Isg15, and Ifit3*) for Real-time PCR quantification. The Real-time PCR was conducted in three biological replicates. *Gapdh* served as an internal control for gene expression analysis. PCR primers and corresponding melting temperatures were shown as follows:

Gapdh, Forward: GAAGGGCTCATGACCACAGT (63.9 °C).
Reverse: GGATGCAGGGATGATGTTCT (61.8 °C).
Mx1, Forward: CCTCCCACATCTGTAAATCACTG (62.5 °C).
Reverse: CGGTTTCCTGTGCTTGTATCA (62.6 °C).
Isg15, Forward: GGAACGAAAGGGGCCACAGCA (63 °C).
Reverse: CCTCCATGGGCCTTCCCTCGA (63.4 °C).
Ifit3, Forward: CCTACATAAAGCACCTAGATGGC (62.4 °C).
Reverse: ATGTGATAGTAGATCCAGGCGT (62.7 °C).

2.14. Enzyme-linked immunosorbent assay for interferon-β

BMDMs were seeded into 12-well plates at a density of 2×10^5 cells per well. After 3'2'-cGAMP or 2'3'-cGAMP stimulation, the secreted interferon-β (IFN-β) in the culture medium was analyzed with the enzyme-linked immunosorbent assay (ELISA) kit (4 A Biotech, #CME0116) according to the manufacturer's instruction.

2.15. Western blot

The western blot experiment was performed according to [27,40]. In brief, BMDMs from 6-well plates were lysed in RIPA buffer supplemented with a complete protease inhibitor cocktail (Sigma). A total of protein of 20–30 μg was loaded on SDS-PAGE gels and separated using electrophoresis. The separated proteins were then electrically transferred to a PVDF membrane. Immunoblot was probed with the indicated antibodies. The protein bands were visualized using a SuperSignal West Pico chemiluminescence ECL kit (Pierce) with the Bio-Rad chemiDoc system.

2.16. Antibodies

The antibodies used for western blot were as follows: anti-STING (#50494), anti-IRF3 (#4302S), anti-Phospho-IRF3(#4947), anti-Phospho-TBK1(#5483S) from Cell Signaling Technology, and anti-TBK1 (#ab40676) from Abcam.

2.17. Figure plotting

We used Perl (v5.18.4), R (v4.3.2), and GraphPad Prisim software for Figure plotting.

2.18. Data Records

All original RNA-Seq data have been deposited in the GEO database with accession number: GSE240884.

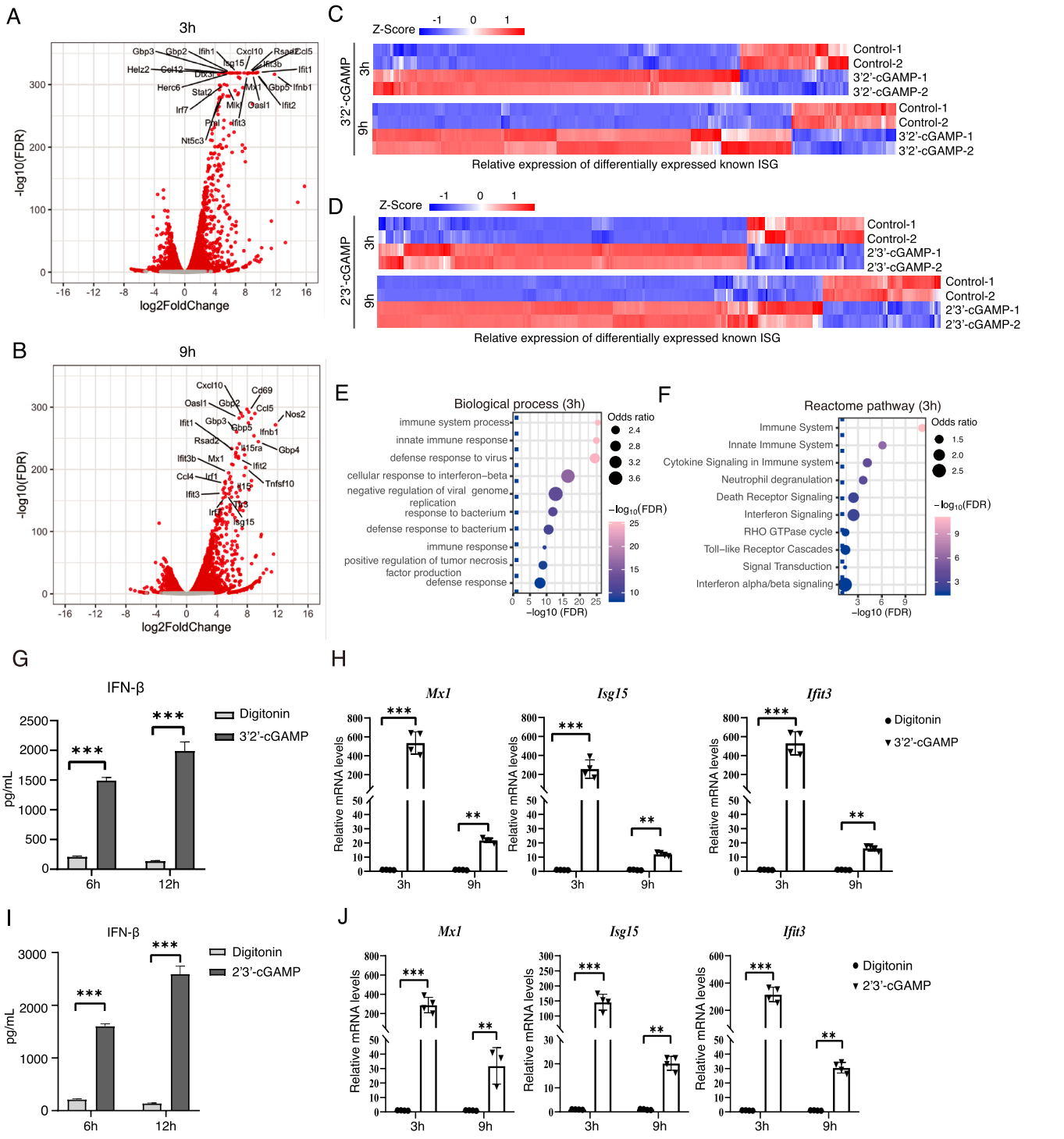

Fig. 2. 3'2'-cGAMP signaling induced strong immune responses in mouse BMDMs. (A-B) Volcano plots showing differentially expressed genes (FDR < 0.05, in red) after 3'2'-cGAMP stimulation at 3 h (A) and 9 h (B). Known ISGs among the top 50 upregulated genes are labeled. (C) Heatmap of differentially expressed interferon-stimulated genes (ISGs) after 3'2'-cGAMP stimulation at 3 h (top) and 9 h (bottom). (D) Heatmap of differentially expressed ISGs after 2'3'-cGAMP stimulation at 3 h (top) and 9 h (bottom). (E-F) Enriched GO biological processes (E) and Reactome pathways (F) of upregulated genes after 3'2'-cGAMP stimulation at 3 h. (G) IFN-β levels in digitonin-permeabilized BMDMs with or without 3'2'-cGAMP stimulation at 6 and 12 h, measured by ELISA. (H) qPCR analysis of known ISGs, including *Mx1*, *Isg15*, and *Ifit3*, in digitonin-permeabilized BMDMs with or without 3'2'-cGAMP stimulation at 3 and 9 h. (I) IFN-β levels in digitonin-permeabilized BMDMs with or without 2'3'-cGAMP stimulation at 6 and 12 h, measured by ELISA. (J) qPCR analysis of known ISGs, including *Mx1*, *Isg15*, and *Ifit3*, in digitonin-permeabilized BMDMs with or without 2'3'-cGAMP stimulation at 3 and 9 h.

3. Results

3.1. Overview of experimental design and RNA-Seq profiling

To investigate potential immune responses mediated by 3'2'-cGAMP signaling in mammals, we collected primary macrophage cells (bone marrow-derived macrophages, BMDMs) from mice and performed RNA-Seq experiments after treating digitonin permeabilized BMDMs with or without 3'2'-cGAMP or canonical 2'3'-cGAMP at 3 h (3 h) and 9 h (9 h) (Fig. 1A, Materials and Methods). In parallel, we collected BMDMs from *Sting*-deficient mice and performed the same experimental procedure to investigate the dependency of 3'2'-cGAMP signaling on STING (Fig. 1A). To measure the transcriptome changes more precisely, we performed the experiments in biological replicates for each treatment, resulting in a total of twenty-four RNA-Seq samples (Fig. 1A). The RNA-Seq data were of high quality, as demonstrated by uniformly distributed reads without 3' bias across the gene body of annotated genes (Fig. 1B) and highly similar distributions of read G+C content across all samples (Fig. 1C). We obtained approximately 20.2 million mapped reads per sample (Fig. 1D) and reliably quantified more than 14,000 protein-coding genes per sample on average (Fig. 1E), which were quite similar across samples of 3'2'-cGAMP or 2'3'-cGAMP stimulated WT and *Sting*-deficient BMDMs (Supplementary Tables S1, 2), enabling largely unbiased comparison between 3'2'-cGAMP signaling and 2'3'-cGAMP signaling. Notably, the gene expression abundance between biological replicates was highly correlated (Fig. 1F, Supplementary Fig. S1A), demonstrating the experiments' validity. The principal component analysis (PCA) showed that the first two principal components (PC) explained up to 83.8 % of total expression variance in 3'2'-cGAMP and 2'3'-cGAMP stimulated WT BMDMs (Fig. 1B). The digitonin permeabilized BMDMs without 3'2'-cGAMP or 2'3'-cGAMP stimulation (mock control) were well separated from 3'2'-cGAMP or 2'3'-cGAMP stimulated samples by the second PC (PC2) in WT BMDMs (Fig. 1B), but this separation was not observed in *Sting*-deficient BMDMs (Supplementary Fig. S1B). Additionally, PCA analysis indicated comparable effects of 3'2'-cGAMP and 2'3'-cGAMP stimulation on the transcriptome changes (Fig. 1B). Together, these results demonstrated the high quality of the RNA-Seq data and indicated a marked effect of 3'2'-cGAMP signaling activation on the gene expression changes in mouse immune cells.

3.2. 3'2'-cGAMP signaling induces strong immune responses in mouse BMDMs

We further analyzed the transcriptome data to investigate whether 3'2'-cGAMP signaling induces immune responses in BMDMs. Consistent with PCA analysis results, the activation of 3'2'-cGAMP signaling led to substantial alternations of gene expression in WT BMDMs, with 5877 and 6385 differentially expressed genes identified after 3'2'-cGAMP stimulation compared with corresponding mock control at 3 h and 9 h, respectively (Fig. 2A-B, Supplementary Tables S3,4). Of the top 50 differentially upregulated genes, over 46 % were known interferon-stimulated genes (ISGs), including *Cxcl10*, *Ifit3*, *Mx1*, and *Isg15* (Fig. 2A-B). Consistently, more than 76 % of differentially expressed ISGs were upregulated at 3 h or 9 h after 3'2'-cGAMP signaling activation (Fig. 2 C), closely resembling the response to 2'3'-cGAMP signaling activation (Fig. 2D, Supplementary Fig. S2). Additionally, gene ontology and Reactome pathway enrichment analysis showed that upregulated genes were significantly enriched in the innate immune-related biological processes and pathways, such as innate immune response, defense response to virus, cellular response to interferon-beta, innate immune system, cytokine signaling in immune system, and interferon signaling (Fig. 2D-E, Supplementary Fig. S3, Supplementary Table S7). Furthermore, more than 81 % of upregulated genes following 3'2'-cGAMP stimulation at 3 h were also significantly increased following 2'3'-cGAMP stimulation at 3 h. At 9 h, this overlap increased to 93 % (Supplementary Tables S3–6). These results indicate that the activation of 3'2'-cGAMP signaling induces a robust innate immune gene signature in mouse macrophages, comparable to that induced by canonical CDN 2'3'-cGAMP stimulation. To further confirm these results, we measured the abundance of IFN-β and traditional ISGs in digitonin permeabilized BMDMs with and without 3'2'-cGAMP stimulation using ELISA and q-PCR. The results showed that IFN-β was significantly induced by 3'2'-cGAMP signaling activation at 6 h and 12 h (Fig. 2 G). Moreover, typical ISGs, including *Mx1*, *Isg15*, and *Ifit3*, were also strongly upregulated at 3 h and 9 h (Fig. 2H), comparable to that following 2'3-cGAMP signaling activation (Fig. 2I-J). Together, these results demonstrate that 3'2'-cGAMP signaling induces robust immune responses in mouse immune cells.

3.3. 3'2'-cGAMP signaling mediated immune responses are mostly STING dependent

The 3'2'-cGAMP exerts antiviral effects by activating the STING homolog in *Drosophila* [22]. We then investigated the dependency between 3'2'-cGAMP signaling and STING in mice. The PCA results in digitonin permeabilized BMDMs of *Sting*-deficient mice showed that 3'2'-cGAMP stimulated samples clustered with digitonin-permeabilized mock controls (Supplementary Fig. S1B), indicating that STING has a strong effect on 3'2'-cGAMP-mediated immune responses. Consistently, the differentially upregulated genes identified after 3'2'-cGAMP signaling activation identified in WT BMDMs (3'2'-cGAMP induced genes) displayed a similar distribution of expression alteration compared to all expressed genes in *Sting*-deficient BMDMs after 3'2'-cGAMP stimulation at 3 h and 9 h (Fig. 3 A, B). Furthermore, no significant correlation of expression changes of the 3'2'-cGAMP signaling-induced genes was observed between WT and *Sting*-deficient BMDMs at 3 h and 9 h post 3'2'-cGAMP signaling activation (Fig. 3 C, D), which was further confirmed based on 1000 simulation analyses (Supplementary Fig. S4). These results indicate that 3'2'-cGAMP-mediated immune responses are strongly dependent on STING. In line with this finding, STING deficiency abolished the induction of IFN-β following 3'2'-cGAMP stimulation, as measured by ELISA (Fig. 3E). Western blot experiments consistently showed that the ablation of STING reduced the 3'2'-cGAMP signaling activation-induced phosphorylation of TBK1 and IRF3, similar to effects observed after 2'3'-cGAMP stimulation (Fig. 3 F). Together, the above results demonstrated that 3'2'-cGAMP signaling mediated immune responses in mice were largely STING dependent.

3.4. 3'2'-cGAMP signaling elicits several distinct cellular programs compared with 2'3'-cGAMP signaling

After establishing the role of 3'2'-cGAMP signaling in STING-dependent immune responses, we then performed a comparative transcriptome analysis to investigate the differences between 3'2'-cGAMP signaling and 2'3'-cGAMP signaling mediated immune responses. We identified 219 differentially expressed (DE) genes between 3'2'-cGAMP signaling and 2'3'-cGAMP signaling by directly comparing their stimulated transcriptomes (Supplementary Table S8). Notably, compared to 2'3'-cGAMP signaling, most DE genes (200 out of 219, 91 %) were upregulated at 3 h post 3'2'-cGAMP signaling activation. We then examined whether these 200 upregulated DE genes were due to subtle differences in activation timing between 3'2'-cGAMP signaling and 2'3'-cGAMP signaling. The result showed that 113 out of the 200 upregulated DE genes were also significantly induced following 2'3-cGAMP signaling activation at 9 h compared to mock control, indicating that the activation timing difference may explain 56.5 % of these 200 upregulated DE genes. The remaining 87 DE genes were upregulated explicitly following 3'2-cGAMP signaling activation compared to both 2'3-cGAMP signaling activation and mock control. Moreover, analysis of public RNA-Seq data confirmed that none of these 87 upregulated DE genes were significantly induced by 2'3'-cGAMP stimulation. We designated these 87

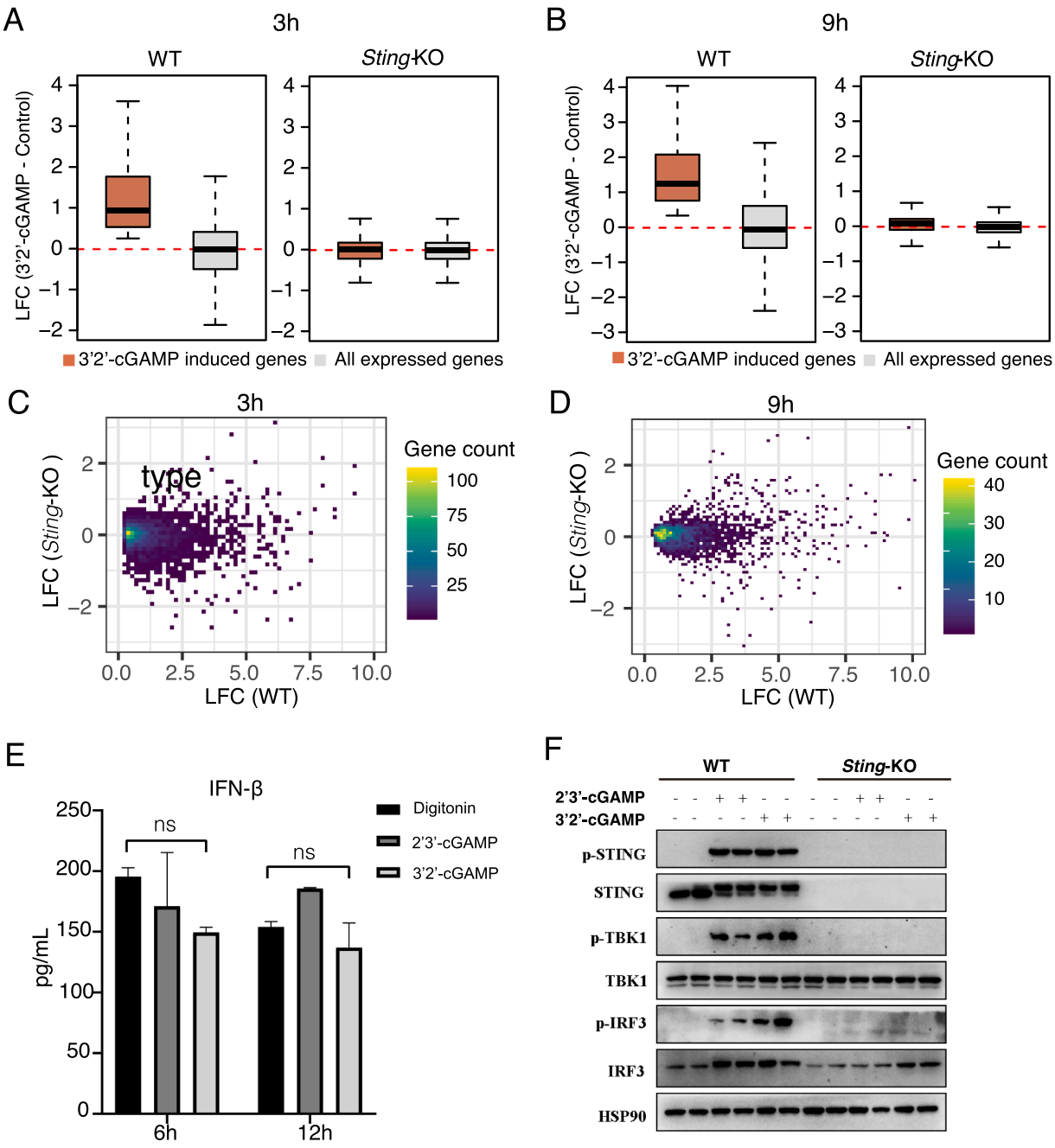

Fig. 3. 3'2'-cGAMP signaling mediated immune responses were predominantly STING dependent. (A-B) Box plots showing expression fold-changes in log2 scale (LFC) for genes induced by 3'2'-cGAMP signaling in WT (left) and STING-deficient (right) BMDMs at 3 h (A) and 9 h (B). (C-D) Correlation of expression changes in log2 scale (LFC) for genes induced by 3'2'-cGAMP signaling between WT and *Sting*-deficient BMDMs at 3 h (C) and 9 h (D). (E) IFN-β protein levels in STING-deficient BMDMs after 3'2'-cGAMP or 2'3'-cGAMP stimulation at 6 and 12 h, measured by ELISA. (F) Western blot analysis of STING, TBK1, IRF3, phosphorylated STING (p-STING), phosphorylated TBK1 (p-TBK1), and phosphorylated IRF3 (p-IRF3) in WT and *Sting*-deficient BMDMs after 3'2'-cGAMP or 2'3'-cGAMP stimulation at 3 h.

upregulated DE genes as "3'2'-cGAMP signaling preferentially induced genes" (Supplementary Table S9). After ranking 3'2'-cGAMP signaling preferentially induced genes based on differential expression fold changes, we found that 13 out of the top 20 upregulated DE genes were nucleosome-related genes (Fig. 4 A). Consistently, gene ontology enrichment analysis showed that 3'2'-cGAMP signaling preferentially induced genes were highly enriched in nucleosome-related functions, particularly nucleosome positioning and assembly (Fig. 4B, C, Supplementary Table S10). Notably, 3'2'-cGAMP signaling preferentially induced genes were not randomly distributed but enriched on chromosome 13 (Fig. 4D). Intriguingly, 10 out of 15 upregulated DE genes on chromosome 13 were nucleosome-related, mostly located within a large histone gene cluster (Fig. 4E, Supplementary Table S10). In addition to nucleosome genes, we found significant enrichment of genes involved in transcriptional regulation, particularly transcription factors, among the 3'2'-cGAMP signaling preferentially induced genes (Fig. 4A-C). These transcription factors belong to several transcription factor complexes, such as the AP-1 complex, which includes *Fos*, *Jun*, and *Jund* genes. Protein-protein interaction (PPI) analysis further indicated that these transcription factors from different transcription factor families formed a dense transcription factors network with significantly more PPI than expected by chance (Fig. 4 F, observed edges: 88, expected edges: 26, $p < 1.0e\text{-}15$). These results indicate that 3'2'-cGAMP signaling specifically induces many genes functioning in the nucleus for chromatin and

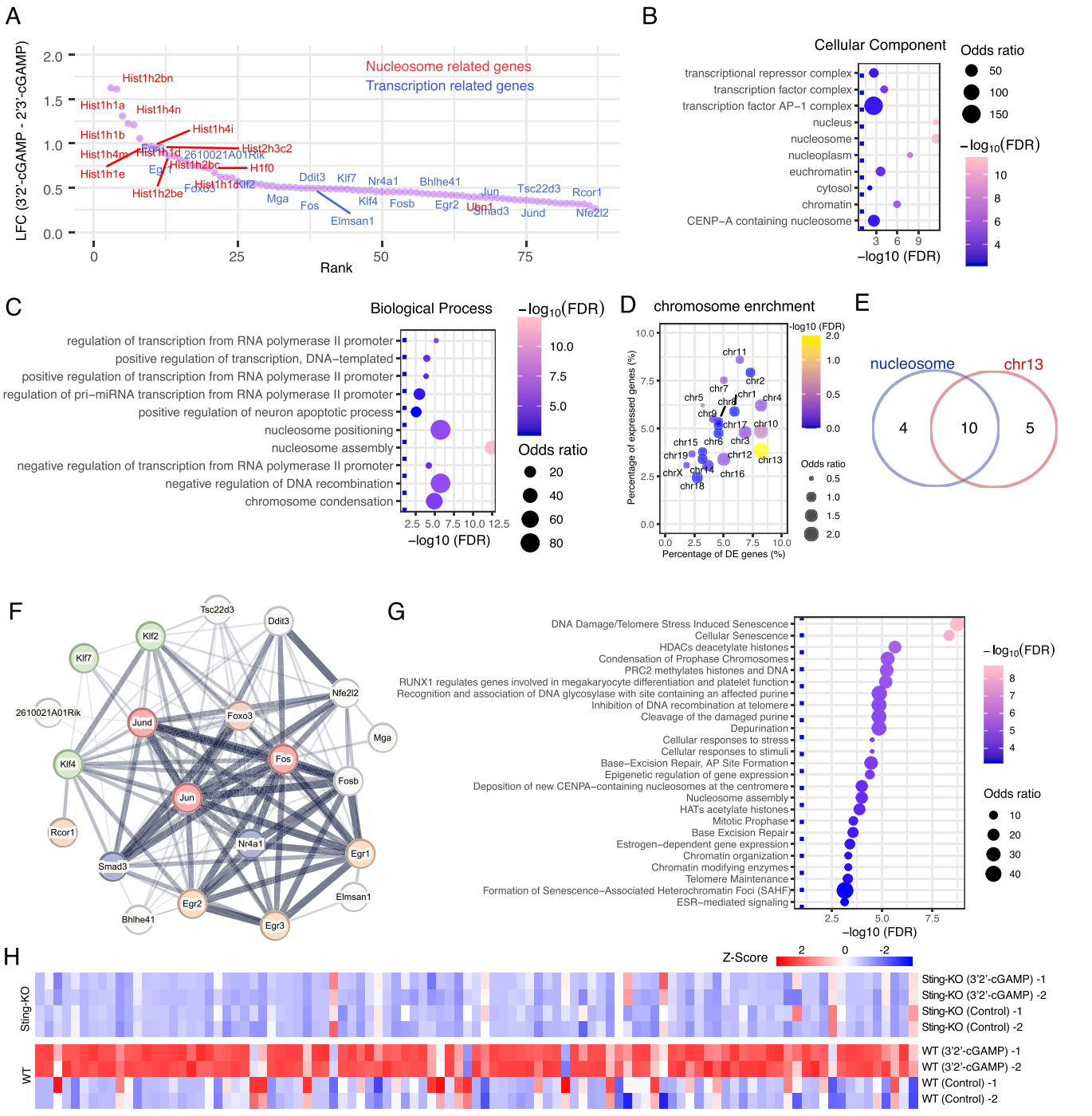

Fig. 4. 3'2'-cGAMP signaling triggers several distinct cellular programs compared with 2'3'-cGAMP signaling. (A) List of genes specifically induced by 3'2'-cGAMP signaling, ranked by log2-fold changes (LFC) between 3'2'-cGAMP and 2'3'-cGAMP stimulation. Nucleosome-related genes are labeled in red, and transcription-related genes in blue. (B-C) Top 10 enriched GO terms for Cellular Components (B) and Biological Processes (C) among genes specifically induced by 3'2'-cGAMP signaling. (D) Chromosome loci enrichment analysis of 3'2'-cGAMP-induced genes, compared to all expressed genes. (E) Venn diagram illustrating overlaps between genes specifically induced by 3'2'-cGAMP signaling in the chr13-A3.1 region, nucleosome-related genes, and genes located on chr13. (F) Protein-protein interaction (PPI) network of transcription factors specifically induced by 3'2'-cGAMP signaling. Transcription factors are color-coded by family identity. (G) Top 20 enriched Reactome pathways for genes specifically induced by 3'2'-cGAMP signaling. (H) Heatmap showing the expression abundance of 3'2'-cGAMP-specific genes in WT and STING-deficient BMDMs before and after 3'2'-cGAMP stimulation.

transcriptional regulation, potentially affecting diverse biological processes. Consistently, we found that 3'2'-cGAMP preferentially induced DE genes were significantly enriched in several fundamental pathways, such as epigenetic regulation of gene expression and cellular senescence (Fig. 4 G). Notably, the comparison of gene expression profiling between WT and *Sting*-deficient digitonin-permeabilized BMDMs before and after 3'2'-cGAMP stimulation showed that most of these 3'2'-cGAMP preferentially induced DE genes were STING-dependent (Fig. 4H). Together, the above results indicate that 3'2'-cGAMP signaling preferentially elicited many STING-dependent genes involved in transcription and nucleosome positioning and assembly in the nucleus, eliciting several distinct cellular programs compared with 2'3'-cGAMP signaling.

3.5. Potential adverse effects of 3'2'-cGAMP signaling activation

The use of adjuvant increases the risk of developing autoimmune or autoinflammatory syndromes, such as SLE[41–43]. To investigate whether 3'2'-cGAMP signaling activation might be associated with adjuvant-induced autoimmune or autoinflammatory side effects, we analyzed blood transcriptome data from three independent SLE cohorts, measuring expression changes of 3'2'-cGAMP signaling-induced genes

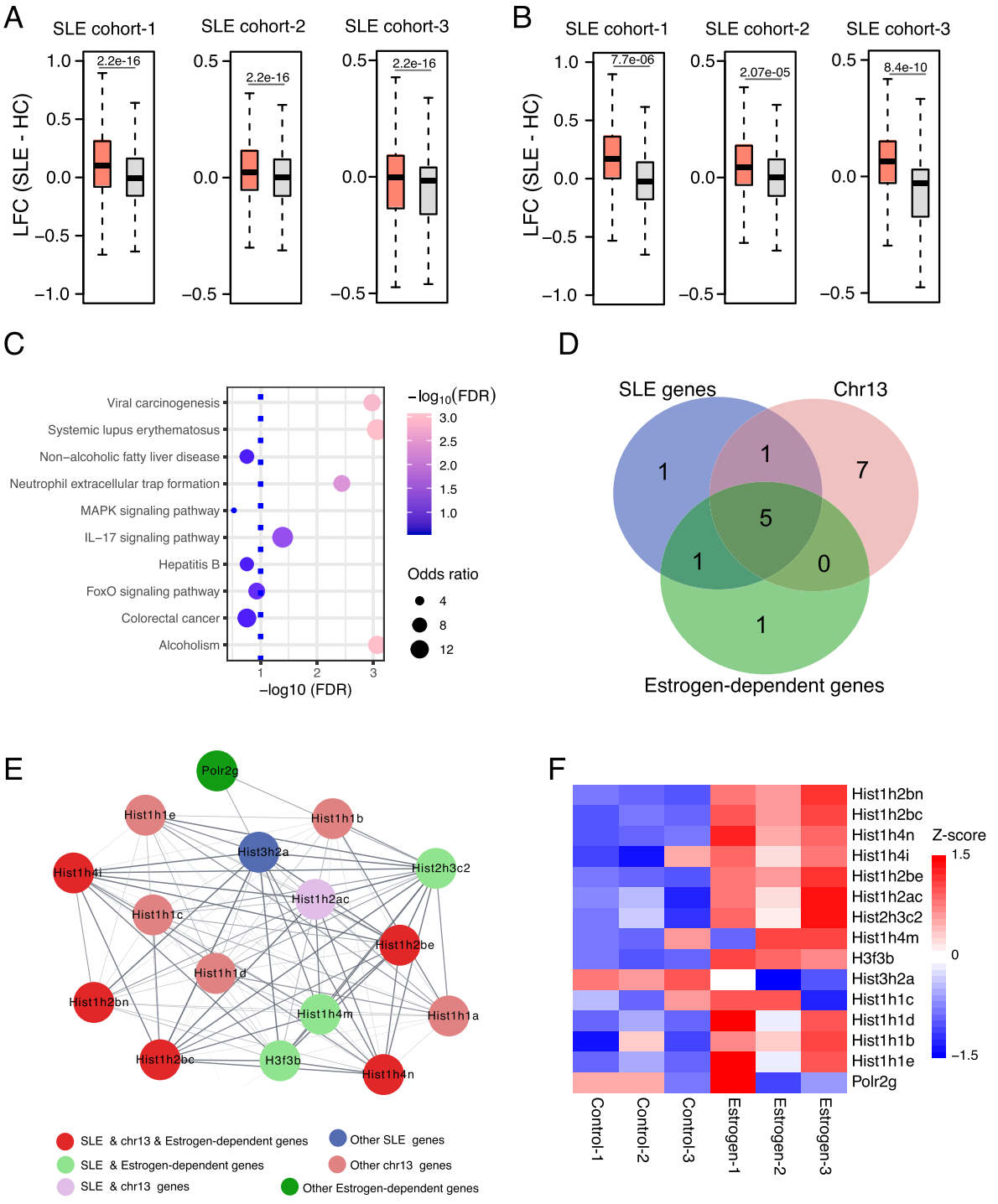

Fig. 5. The association between 3'2'-cGAMP signaling and SLE. (A) Boxplot showing fold-change expression (log2-scale, LFC) of 3'2'-cGAMP signaling-induced genes in SLE patients compared to healthy donors, based on RNA-Seq data from three SLE cohorts (SLE cohort-1, SLE cohort-2, SLE cohort-3). (B) Boxplot showing fold-change expression (log2-scale, LFC) of genes specifically induced by 3'2'-cGAMP signaling in SLE patients versus healthy donors, based on RNA-Seq data from the three SLE cohorts. (C) Top 10 enriched KEGG pathways for genes specifically induced by 3'2'-cGAMP signaling. (D-E) Venn diagrams showing overlaps between genes specifically induced by 3'2'-cGAMP signaling in systemic lupus erythematosus pathways (SLE genes), genes in the Chr13-A3.1 region (Chr13-A3.1 genes), and genes in the estrogen-dependent gene expression Reactome pathway (Estrogen-dependent genes). (F) Protein-protein interaction (PPI) network of the union genes from the SLE, Chr13-A3.1, and estrogen-dependent gene groups. Genes are color-coded based on their overlap status. (G) Heatmap showing expression levels of union genes from the SLE, Chr13-A3.1, and estrogen-dependent gene groups in estrogen-treated versus mock control conditions in the mouse raw 264.7 macrophage cell line.

in SLE patients. The result showed that 3'2'-cGAMP signaling-induced genes were significantly upregulated compared to all expressed genes in all three independent SLE cohorts (Wilcoxon rank sum test, adjusted $p < 0.05$, Fig. 5A). The upregulation magnitude in SLE patients was more pronounced for 3'2'-cGAMP signaling preferentially induced genes than for total 3'2'-cGAMP signaling induced genes (Fig. 5A, B). KEGG pathway enrichment analysis showed that 3'2'-cGAMP signaling preferentially induced genes were significantly enriched in the SLE pathway (Fig. 5C, Supplementary Tables S10). Additionally, neutrophil extracellular trap formation, which plays a critical role in the pathogenesis of SLE [44], was also enriched (Fig. 5C). We further investigated these 3'2'-cGAMP signaling preferentially induced genes that participated in the SLE pathway in more detail. Intriguingly, we found that more than half of the annotated SLE genes in the 3'2'-cGAMP signaling preferentially induced gene list were located on chromosome 13, all of which were nucleosome-related. Moreover, these overlapping nucleosome-related genes were primarily regulated by estrogen (Fig. 5D), a steroid hormone associated with female reproductive organs [45,46]. Estrogen is generally thought to enhance immune response and accelerate SLE development and pathogenesis [45,46]. Importantly, we found the SLE pathway genes, nucleosome genes on chromosome 13, and estrogen-dependent genes in the 3'2'-cGAMP signaling preferentially induced gene list were strongly interconnected (Fig. 5E, observed edges:87, expected edges:14, $p < 1.0e-16$), the majority of which were significantly responsive to estrogen treatment in mouse macrophage cell lines (Fig. 5F). Together, these results indicate an association between 3'2'-cGAMP signaling activation and autoimmune disease SLE, suggesting potential adverse effects of using 3'2'-cGAMP as an adjuvant that should be monitored.

4. Discussion

The cGAS-STING pathway is a promising target for antiviral vaccines and cancer immunotherapy [3,11,12]. Bacterial CDNs, such as c-di-GMP and c-di-AMP, along with the mammalian CDN 2'3'-cGAMP, show strong potential as immune adjuvants in anticancer and antiviral vaccine therapies [12–21]. However, the known natural CDNs are generally susceptible to nuclease degradation [47]. Thus, there is a strong need to evaluate newly identified CDNs for their potential as adjuvants. 3'2'-cGAMP is a recently identified, nuclease-resistant CDN in *Drosophila* and bacteria that protects against viral infection in *Drosophila melanogaster* [22]. In this study, we conducted a comparative transcriptome study to characterize the potential immune responses triggered by 3'2'-cGAMP in mammalian immune cells. The experimental design and RNA-Seq profiling in this study provided comprehensive insights into the immune responses mediated by 3'2'-cGAMP signaling in mouse primary macrophage cells. The data analysis showed that 3'2'-cGAMP signaling activation significantly impacted gene expression in mouse immune cells, especially by inducing robust innate immune responses, including IFN-β induction and upregulation of ISGs such as *Isg15*, *Mx1*, and *Ifit3* [10]. The transcriptome comparison between 3'2'-cGAMP and canonical mammalian 2'3'-cGAMP signaling highlighted the potency of 3'2'-cGAMP in inducing immune responses comparable to 2'3'-cGAMP. This finding demonstrates 3'2'-cGAMP's effectiveness in eliciting immune signatures, suggesting its potential as an alternative or complementary immune-stimulating agent in antiviral vaccines and cancer immunotherapy. STING is an essential adaptor protein in the cGAS-STING pathway, regulating DNA-mediated, type I interferon-dependent innate immunity [6]. The dependency of 3'2'-cGAMP signaling on STING was a key finding, affirming the crucial role of STING in mediating the immune responses triggered by 3'2'-cGAMP in mammals. The association between 3'2'-cGAMP signaling and STING, shown through gene expression changes and loss of immune response in *Sting*-deficient macrophages, underscores STING's significance in orchestrating 3'2'-cGAMP-mediated immune cascades.

Although we found that immune responses triggered by both 3'2'-cGAMP and 2'3'-cGAMP signaling were primarily STING-dependent, comparative transcriptome analysis revealed distinctive cellular programs initiated by 3'2'-cGAMP signaling. While both 3'2'-cGAMP and 2'3'-cGAMP signaling activated strong type I interferon-dependent innate immunity, 3'2'-cGAMP signaling activation launched a unique landscape of gene regulation in the nucleus compared to 2'3'-cGAMP signaling, particularly in nucleosome-related genes and transcriptional regulation factors. This divergence highlights specific functions and pathways influenced by 3'2'-cGAMP, suggesting novel mechanisms for immune regulation and cellular homeostasis. In this study, we found that 3'2'-cGAMP signaling specifically activated many STING-dependent genes involved in transcriptional regulation, including those forming the AP-1 complex, which comprises *Fos*, *Jun*, and *Jund*. As broadly expressed pioneer factors [48,49], AP-1 complex members respond to diverse stimuli and are linked to age-related pathologies and phenotypes [50,51]. A more recent study found that AP-1-linked chromatin opening drives organismal maturation by disrupting cell identity TFBS-rich *cis*-regulatory elements, thereby reprogramming transcriptome and cell function, a mechanism hijacked in aging through ongoing chromatin opening in mice [52]. AP-1 is also chronically active in a subset of glial cells in aging *Drosophila* brains, contributing to a senescent phenotype [53]. Notably, the STING pathway plays a critical role in mediating cellular senescence in human tissues [54]. These observations suggest that 3'2'-cGAMP signaling activation mediated AP-1 complex induction may participate in cellular senescence. Thus, future studies should pay attention to the process of cellular senescence in the development of 3'2'-cGAMP-based adjuvants.

While adjuvants are beneficial for antiviral vaccines and cancer immunotherapy, their potential side effects must be closely monitored. Indeed, adjuvants increase the risk of developing autoimmune syndromes, including systemic lupus erythematosus (SLE) [41–43]. Our transcriptome analysis offers an unbiased investigation of the potential side effects of using 3'2'-cGAMP as an adjuvant. We detected an association between 3'2'-cGAMP signaling and autoimmune disease SLE by analyzing transcriptome data from several independent SLE cohorts. Notably, this association was primarily driven by nucleosome-related genes clustered on chromosome 13. Nucleosomes are major autoantigens in systemic lupus erythematosus, circulating as complexes in patients' sera, and appear to play a key role in disease development [55,56]. These results suggest that the use of 3'2'-cGAMP as an adjuvant may have potential side effects, which should be monitored, possibly by assessing the abundance of nucleosome-related genes on chromosome 13 in the blood.

The 3'2'-cGAMP has been identified in both Drosophila and bacteria, but its presence in mammalian species has not been thoroughly investigated. The upregulation of 3'2'-cGAMP signaling-induced genes in SLE cohorts, particularly those associated with nucleosome-related genes and estrogen-responsive genes, suggests a potential link between 3'2'-cGAMP signaling, nucleosome regulation, estrogen, and the pathogenesis of SLE. Both nucleosome and estrogen have been linked to SLE pathogenesis [37,55]. If 3'2'-cGAMP is found to exist in mammalian species, our findings could open new avenues for investigating its role in autoimmune diseases, particularly those involving type I interferon pathways.

This study has several limitations: (1) Gender-based research highlights sex differences in biological processes, clinical disorders and pharmacological interventions [57–59]. Previous studies have shown that gender affects immune responses [60,61]. Our study only included male mice, so it remains unclear whether sex-specific differences influence immune responses following 3'2'-cGAMP signaling activation. (2) Although we observed significant gene expression differences induced by 3'2'-cGAMP signaling compared to 2'3'-cGAMP signaling, the underlying mechanism requires further investigation, possibly by comparing the crystal structures of the STING-3'2'-cGAMP and STING-2'3'-cGAMP complexes.

5. Conclusion

In conclusion, our results demonstrated the significant impact of 3'2'-cGAMP signaling on immune responses in mammalian immune cells, highlighting its STING-dependent effects, immune characteristics, and potential adverse effects. These findings may aid in the development of 3'2'-cGAMP-based adjuvants for antiviral vaccines and cancer immunotherapy.

Author Contributions

H.H., Z.H. and C.W conceptualized this study; Y.G., M.M., G.X., S.C. and X.Z. performed experiments; G.X., M.M., and J.H. performed data analysis, data visualization, and data curation; H.H., Z.H. and C.W acquired funding for this study. H.H. wrote the original draft with contributions from all authors.

Funding

Dr. Haiyang Hu was supported by the National Key Research and Development Program of China (2022YFC2303200, 2021YFF0702003), the National Natural Science Foundation of China (82471347), the Natural Science Foundation of Chongqing (CSTB2022NSCQ-MSX1114). Dr. Ze Hong was supported by the National Natural Science Foundation of China (82473930, 82204408). Dr. Chen Wang was supported by the National Key Research and Development Program of China (2022YFC2303200, 2021YFF0702003).

CRediT authorship contribution statement

Yan Gao: Formal analysis, Data curation. **Haiyang Hu:** Writing – review & editing, Writing – original draft, Validation, Supervision, Resources, Funding acquisition, Formal analysis, Conceptualization. **Ze Hong:** Supervision, Resources, Funding acquisition, Conceptualization. **Chen Wang:** Resources, Funding acquisition, Conceptualization. **Jiameng Hu:** Formal analysis. **Xiang Zhang:** Resources, Project administration. **Saihua Chen:** Methodology. **Munire Maimaiti:** Methodology, Formal analysis, Data curation. **Gucheng Xu:** Validation, Formal analysis, Data curation.

Declaration of Competing Interest

The authors declare that they have no known competing financial interests or personal relationships that could have appeared to influence the work reported in this paper.

Appendix A. Supporting information

Supplementary data associated with this article can be found in the online version at doi:10.1016/j.csbj.2024.11.021.

References

[1] Zhang ZD, Zhong B. Regulation and function of the cGAS-MITA/STING axis in health and disease. Cell Insight 2022;1(1):100001.
[2] Hopfner KP, Hornung V. Molecular mechanisms and cellular functions of cGAS-STING signalling. Nat Rev Mol Cell Biol 2020;21(9):501–21.
[3] Zhou M, Tang Y, Xu W, Hao X, Li Y, Huang S, Xiang D, Wu J. Bacteria-based immunotherapy for cancer: a systematic review of preclinical studies. Front Immunol 2023;14:1140463.
[4] Yu X, Cai L, Yao J, Li C, Wang X. Agonists and Inhibitors of the cGAS-STING Pathway. Molecules 2024;29(13).
[5] Romling U, Galperin MY, Gomelsky M. Cyclic di-GMP: the first 25 years of a universal bacterial second messenger. Microbiol Mol Biol Rev 2013;77(1):1–52.
[6] Ishikawa H, Ma Z, Barber GN. STING regulates intracellular DNA-mediated, type I interferon-dependent innate immunity. Nature 2009;461(7265):788–92.
[7] Gulen MF, Koch U, Haag SM, Schuler F, Apetoh L, Villunger A, Radtke F, Ablasser A. Signalling strength determines proapoptotic functions of STING. Nat Commun 2017;8(1):427.
[8] Li C, Liu W, Wang F, Hayashi T, Mizuno K, Hattori S, Fujisaki H, Ikejima T. DNA damage-triggered activation of cGAS-STING pathway induces apoptosis in human keratinocyte HaCaT cells. Mol Immunol 2021;131:180–90.
[9] Zhang D, Liu Y, Zhu Y, Zhang Q, Guan H, Liu S, Chen S, Mei C, Chen C, Liao Z, et al. A non-canonical cGAS-STING-PERK pathway facilitates the translational program critical for senescence and organ fibrosis. Nat Cell Biol 2022;24(5):766–82.
[10] Maimaiti M, Li C, Cheng M, Zhong Z, Hu J, Yang L, Zhang L, Hong Z, Song J, Pan M, et al. Blocking cGAS-STING pathway promotes post-stroke functional recovery in an extended treatment window via facilitating remyelination. Med 2024;5(6):622–44. e628.
[11] Gutjahr A, Papagno L, Nicoli F, Kanuma T, Kuse N, Cabral-Piccin MP, Rochereau N, Gostick E, Lioux T, Perouzel E, et al. The STING ligand cGAMP potentiates the efficacy of vaccine-induced CD8+ T cells. JCI Insight 2019;4(7).
[12] Tian X, Ai J, Tian X, Wei X. cGAS-STING pathway agonists are promising vaccine adjuvants. Med Res Rev 2024;44(4):1768–99.
[13] Gogoi H, Mansouri S, Jin L. The Age of Cyclic Dinucleotide Vaccine Adjuvants. Vaccin (Basel) 2020;8(3).
[14] Van Dis E, Sogi KM, Rae CS, Sivick KE, Surh NH, Leong ML, Kanne DB, Metchette K, Leong JJ, Bruml JR, et al. STING-Activating Adjuvants Elicit a Th17 Immune Response and Protect against Mycobacterium tuberculosis Infection. Cell Rep 2018;23(5):1435–47.
[15] Martin TL, Jee J, Kim E, Steiner HE, Cormet-Boyaka E, Boyaka PN. Sublingual targeting of STING with 3'3'-cGAMP promotes systemic and mucosal immunity against anthrax toxins. Vaccine 2017;35(18):2511–9.
[16] Karaolis DK, Newstead MW, Zeng X, Hyodo M, Hayakawa Y, Bhan U, Liang H, Standiford TJ. Cyclic di-GMP stimulates protective innate immunity in bacterial pneumonia. Infect Immun 2007;75(10):4942–50.
[17] Hu DL, Narita K, Hyodo M, Hayakawa Y, Nakane A, Karaolis DK. c-di-GMP as a vaccine adjuvant enhances protection against systemic methicillin-resistant Staphylococcus aureus (MRSA) infection. Vaccine 2009;27(35):4867–73.
[18] Wang J, Li P, Yu Y, Fu Y, Jiang H, Lu M, Sun Z, Jiang S, Lu L, Wu MX. Pulmonary surfactant-biomimetic nanoparticles potentiate heterosubtypic influenza immunity. Science 2020;367(6480).
[19] Chandra D, Quispe-Tintaya W, Jahangir A, Asafu-Adjei D, Ramos I, Sintim HO, Zhou J, Hayakawa Y, Karaolis DK, Gravekamp C. STING ligand c-di-GMP improves cancer vaccination against metastatic breast cancer. Cancer Immunol Res 2014;2(9):901–10.
[20] Karaolis DK, Cheng K, Lipsky M, Elnabawi A, Catalano J, Hyodo M, Hayakawa Y, Raufman JP. 3',5'-Cyclic diguanylic acid (c-di-GMP) inhibits basal and growth factor-stimulated human colon cancer cell proliferation. Biochem Biophys Res Commun 2005;329(1):40–5.
[21] Ohkuri T, Kosaka A, Ishibashi K, Kumai T, Hirata Y, Ohara K, Nagato T, Oikawa K, Aoki N, Harabuchi Y, et al. Intratumoral administration of cGAMP transiently accumulates potent macrophages for anti-tumor immunity at a mouse tumor site. Cancer Immunol Immunother 2017;66(6):705–16.
[22] Slavik KM, Morehouse BR, Ragucci AE, Zhou W, Ai X, Chen Y, Li L, Wei Z, Bahre H, Konig M, et al. cGAS-like receptors sense RNA and control 3'2'-cGAMP signalling in Drosophila. Nature 2021;597(7874):109–13.
[23] Holleufer A, Winther KG, Gad HH, Ai X, Chen Y, Li L, Wei Z, Deng H, Liu J, Frederiksen NA, et al. Two cGAS-like receptors induce antiviral immunity in Drosophila. Nature 2021;597(7874):114–8.
[24] Fatma S, Chakravarti A, Zeng X, Huang RH. Molecular mechanisms of the CdnG-Cap5 antiphage defense system employing 3',2'-cGAMP as the second messenger. Nat Commun 2021;12(1):6381.
[25] Song J, Zhang L, Li C, Maimaiti M, Sun J, Hu J, Li L, Zhang X, Wang C, Hu H. m(6)A-mediated modulation coupled with transcriptional regulation shapes long noncoding RNA repertoire of the cGAS-STING signaling. Comput Struct Biotechnol J 2022;20:1785–97.
[26] Sun J, Li L, Hu J, Gao Y, Song J, Zhang X, Hu H. Time-course RNA-Seq profiling reveals isoform-level gene expression dynamics of the cGAS-STING pathway. Comput Struct Biotechnol J 2022;20:6490–500.
[27] Pan M, Yin Y, Wang X, Wang Q, Zhang L, Hu H, Wang C. Mice deficient in UXT exhibit retinitis pigmentosa-like features via aberrant autophagy activation. Autophagy 2021;17(8):1873–88.
[28] Hu H, Liu JM, Hu Z, Jiang X, Yang X, Li J, Zhang Y, Yu H, Khaitovich P. Recently Evolved Tumor Suppressor Transcript TP73-AS1 Functions as Sponge of Human-Specific miR-941. Mol Biol Evol 2018;35(5):1063–77.
[29] Bolger AM, Lohse M, Usadel B. Trimmomatic: a flexible trimmer for Illumina sequence data. Bioinformatics 2014;30(15):2114–20.
[30] Ewels P, Magnusson M, Lundin S, Kaller M. MultiQC: summarize analysis results for multiple tools and samples in a single report. Bioinformatics 2016;32(19):3047–8.
[31] Kim D, Paggi JM, Park C, Bennett C, Salzberg SL. Graph-based genome alignment and genotyping with HISAT2 and HISAT-genotype. Nat Biotechnol 2019;37(8):907–15.
[32] Liao Y, Smyth GK, Shi W. featureCounts: an efficient general purpose program for assigning sequence reads to genomic features. Bioinformatics 2014;30(7):923–30.
[33] Wang L, Wang S, Li W. RSeQC: quality control of RNA-seq experiments. Bioinformatics 2012;28(16):2184–5.
[34] Robinson MD, McCarthy DJ, Smyth GK. edgeR: a Bioconductor package for differential expression analysis of digital gene expression data. Bioinformatics 2010;26(1):139–40.
[35] Zhang Y, Mikhaylova L, Kobzik L, Fedulov AV. Estrogen-mediated impairment of macrophageal uptake of environmental TiO2 particles to explain inflammatory effect of TiO2 on airways during pregnancy. J Immunotoxicol 2015;12(1):81–91.

[36] Irizarry RA, Bolstad BM, Collin F, Cope LM, Hobbs B, Speed TP. Summaries of Affymetrix GeneChip probe level data. Nucleic Acids Res 2003;31(4):e15.
[37] Kim JW, Kim HA, Suh CH, Jung JY. Sex hormones affect the pathogenesis and clinical characteristics of systemic lupus erythematosus. Front Med (Lausanne) 2022;9:906475.
[38] Wu X, Dao Thi VL, Huang Y, Billerbeck E, Saha D, Hoffmann HH, Wang Y, Silva LAV, Sarbanes S, Sun T, et al. Intrinsic Immunity Shapes Viral Resistance of Stem Cells. Cell 2018;172(3):423–38. e425.
[39] Herrero J, Muffato M, Beal K, Fitzgerald S, Gordon L, Pignatelli M, Vilella AJ, Searle SM, Amode R, Brent S, et al. Ensembl comparative genomics resources. Database (Oxf) 2016;2016.
[40] Pan M, Yin Y, Hu T, Wang X, Jia T, Sun J, Wang Q, Meng W, Zhu J, Dai C, et al. UXT attenuates the CGAS-STING1 signaling by targeting STING1 for autophagic degradation. Autophagy 2023;19(2):440–56.
[41] Seida I, Alrais M, Seida R, Alwani A, Kiyak Z, Elsalti A, Nil Esirgun S, Abali T, Mahroum N. Autoimmune/inflammatory syndrome induced by adjuvants (ASIA): past, present, and future implications. Clin Exp Immunol 2023;213(1):87–101.
[42] Wang M, Gu H, Zhai Y, Li X, Huang L, Li H, Xie Z, Wen C. Vaccination and the risk of systemic lupus erythematosus: a meta-analysis of observational studies. Arthritis Res Ther 2024;26(1):60.
[43] Peng K, Li X, Yang D, Chan SCW, Zhou J, Wan EYF, Chui CSL, Lai FTT, Wong CKH, Chan EWY, et al. Risk of autoimmune diseases following COVID-19 and the potential protective effect from vaccination: a population-based cohort study. EClinicalMedicine 2023;63:102154.
[44] Yu Y, Su K. Neutrophil Extracellular Traps and Systemic Lupus Erythematosus. J Clin Cell Immunol 2013;4.
[45] Merrheim J, Villegas J, Van Wassenhove J, Khansa R, Berrih-Aknin S, le Panse R, Dragin N. Estrogen, estrogen-like molecules and autoimmune diseases. Autoimmun Rev 2020;19(3):102468.
[46] Kanda N, Tsuchida T, Tamaki K. Estrogen enhancement of anti-double-stranded DNA antibody and immunoglobulin G production in peripheral blood mononuclear cells from patients with systemic lupus erythematosus. Arthritis Rheum 1999;42 (2):328–37.
[47] Chang D, Whiteley AT, Bugda Gwilt K, Lencer WI, Mekalanos JJ, Thiagarajah JR. Extracellular cyclic dinucleotides induce polarized responses in barrier epithelial cells by adenosine signaling. Proc Natl Acad Sci USA 2020;117(44):27502–8.
[48] Vierbuchen T, Ling E, Cowley CJ, Couch CH, Wang X, Harmin DA, Roberts CWM, Greenberg ME. AP-1 Transcription Factors and the BAF Complex Mediate Signal-Dependent Enhancer Selection. Mol Cell 2017;68(6):1067–82. e1012.
[49] Biddie SC, John S, Sabo PJ, Thurman RE, Johnson TA, Schiltz RL, Miranda TB, Sung MH, Trump S, Lightman SL, et al. Transcription factor AP1 potentiates chromatin accessibility and glucocorticoid receptor binding. Mol Cell 2011;43(1): 145–55.
[50] Wang L, Zhang S, Han J, Nie X, Qi Y, Han Y, Chen X, He C. Activation of STING Pathway Contributed to Cisplatin-Induced Cardiac Dysfunction via Promoting the Activation of TNF-alpha-AP-1 Signal Pathway. Front Pharm 2021;12:711238.
[51] Byrns CN, Saikumar J, Bonini NM. Glial AP1 is activated with aging and accelerated by traumatic brain injury. Nat Aging 2021;1(7):585–97.
[52] Patrick R, Naval-Sanchez M, Deshpande N, Huang Y, Zhang J, Chen X, Yang Y, Tiwari K, Esmaeili M, Tran M, et al. The activity of early-life gene regulatory elements is hijacked in aging through pervasive AP-1-linked chromatin opening. Cell Metab 2024;36(8):1858–81. e1823.
[53] Byrns CN, Perlegos AE, Miller KN, Jin Z, Carranza FR, Manchandra P, Beveridge CH, Randolph CE, Chaluvadi VS, Zhang SL, et al. Senescent glia link mitochondrial dysfunction and lipid accumulation. Nature 2024;630(8016): 475–83.
[54] Gulen MF, Samson N, Keller A, Schwabenland M, Liu C, Gluck S, Thacker VV, Favre L, Mangeat B, Kroese LJ, et al. cGAS-STING drives ageing-related inflammation and neurodegeneration. Nature 2023;620(7973):374–80.
[55] Decker P, Singh-Jasuja H, Haager S, Kotter I, Rammensee HG. Nucleosome, the main autoantigen in systemic lupus erythematosus, induces direct dendritic cell activation via a MyD88-independent pathway: consequences on inflammation. J Immunol 2005;174(6):3326–34.
[56] Elbagir S, Mohammed NA, Oke V, Larsson A, Nilsson J, Elshafie A, Elagib EM, Nur MAM, Gunnarsson I, Svenungsson E, et al. Anti-histone and anti-nucleosome rather than anti-dsDNA antibodies associate with IFN-induced biomarkers in Sudanese and Swedish Systemic Lupus Erythematosus patients. Rheumatol (Oxf) 2024.
[57] Hagg S, Jylhava J. Sex differences in biological aging with a focus on human studies. Elife 2021;10.
[58] Hong Y, Hu J, Zhang S, Liu J, Yan F, Yang H, Hu H. Integrative analysis identifies region- and sex-specific gene networks and Mef2c as a mediator of anxiety-like behavior. Cell Rep 2024;43(7):114455.
[59] Consideration of sex differences is necessary to achieve health equity. Nat Rev Nephrol 2024;20(1):1.
[60] Klein SL, Flanagan KL. Sex differences in immune responses. Nat Rev Immunol 2016;16(10):626–38.
[61] Wilkinson NM, Chen HC, Lechner MG, Su MA. Sex Differences in Immunity. Annu Rev Immunol 2022;40:75–94.